Synthesis and Characterization of Acrylic Rubber/Silica Hybrid Composites Prepared by Sol-Gel Technique

Abhijit Bandyopadhyay, Anil K. Bhowmick, Mousumi De Sarkar

Rubber Technology Center, Indian Institute of Technology, Kharagpur-721302, India

Received 20 November 2003; accepted 18 March 2004
DOI 10.1002/app.20681
Published online in Wiley InterScience (www.interscience.wiley.com).

ABSTRACT: The organic–inorganic hybrid composites comprising acrylic rubber and silica were synthesized through sol–gel technique at ambient temperature. The composites were generated through the acid-catalyzed hydrolysis and subsequent condensations of inorganic tetraethoxysilane (TEOS) in the organic acrylic rubber (ACM), solvated in tetrahydrofuran. The morphology of the hybrid materials was investigated by using the transmission electron microscope (TEM) and scanning electron microscope (SEM). Transmission electron micrographs revealed that the silica particles, uniformly distributed over the rubber matrix, are of nanometer scale (20–90 nm). The scanning electron micrographs demonstrated the existence of silica frameworks dispersed in the rubber matrix of the hybrid composites. The X-ray silicon mapping also supported that observation. There was no evidence of chemical interaction between the rubber phase and the dispersed inorganic phase, as confirmed from the infrared spectroscopic analysis and solubility measurements. Dynamic mechanical analysis indicated mechanical reinforcements within the hybrid composites. The composites containing *in situ* silica, formed by sol–gel technique, demonstrated superior tensile strengths and tensile modulus values at 300% elongations with increasing proportions of tetraethoxysilane. However, the improvements in physical properties with similar proportions of precipitated silica were not significant. Maximum tensile strength and tensile modulus were obtained when the rubber phase in the hybrid composites was cured with ammonium benzoate and hexamethylenediamine carbamate system, as compared with benzoyl peroxide cured system. Thermal stability of the hybrid composites was not improved appreciably with respect to the virgin rubber specimen. Residue analysis from thermogravimetric study together with infrared spectroscopic analysis indicated the presence of unhydrolyzed tetraethoxysilane in the hybrid composites. J Appl Polym Sci 93: 2579–2589, 2004

Key words: rubber; nanocomposites; mechanical properties

INTRODUCTION

Organic–inorganic hybrid materials are very important for their extraordinary properties, which arise from the synergism between the properties of the respective components. They comprise inorganic networks, homogenously dispersed in organic polymer matrix. The hybrid materials have gained much interest in recent years because of the remarkable changes in properties such as mechanical,[1] thermal,[2–5] electrical,[6] and magnetic[7] compared to the pure organic polymers. The most commonly employed preparation procedure for these hybrid materials is the use of sol–gel process for the formation of the inorganic network involving a hydrolysable alkoxysilane as the precursor material. The unique properties of these materials are their high-optical transparency and superior mechanical reinforcements due to the distribution of nanoscale silica within the matrix.

Correspondence to: M. De Sarkar (moude@rtc.iitkgp.ernet.in).

Journal of Applied Polymer Science, Vol. 93, 2579–2589 (2004)

Over the past two decades, there have been increasing interest in the development of sol–gel technology due to the fact that this procedure produces inorganic network at relatively low temperatures. The basic route leading to this technique is to hydrolyze a multifunctional alkoxysilane that then undergoes self-condensation to form a three-dimensional network[8]

Hydrolysis:

$$Si(OR)_4 \xrightarrow{H^+/H_2O} Si(OH)_4 + 4ROH$$

where R is alkyl group.

Polycondensation:

$$Si(OH)_4 + Si(OH)_4 \rightarrow (OH)_3Si—O—Si(OH)_3 + H_2O$$

These reactions are highly schematic and are not stoichiometrically balanced. The completion of hydrolysis reaction depends on the amount of water added, the type of solvent used, and pH of the medium. Moreover, when this reaction is carried out in the

presence of a polymeric substance, the hydrophilicity of the material has to be kept in mind; otherwise, this may lead to macrophase separations of the basic components. The amount of water and other experimental conditions have to be chosen in such a way that would allow a wide range of compositional variations in the composites without sacrificing the advantageous points of the process.

Wei et al. demonstrated the formation of transparent hybrid composites based on methyl methacrylate and *in situ* silica.[9,10] Styrene/silica[11] or acrylonitrile/silica[12] hybrid systems, prepared by using sol-gel techniques, form homogeneous hybrid composites without additional covalent bond formation, but with hydrogen bonding as the main interaction at the organic–inorganic interface. Mark et al. observed reinforcement of silicone rubber by using the same technique.[13] Silica is used extensively in the rubber industry as a reinforcing filler.[14] However, the action of silica formed *in situ* by sol–gel technique on the physical properties of commercially available rubbers was not extensively reported. The present work elucidates the synthesis of hybrid composites involving acid catalyzed hydrolysis and condensation of tetraethoxysilane in the presence of acrylic rubber matrix in a solution phase, separately without curing and curing the rubber phase. The structure–property relationship in the hybrids has been established. Comparative studies on the properties of composites prepared by using acrylic rubber and the *in situ* generated silica as well as with the precipitated silica was also conducted.

EXPERIMENTAL

Materials

Acrylic rubber (ACM, Nipol AR51, density at 25°C = 1100 kg/cm^3, Mooney viscosity, ML_{1+4} at 100°C = 51) was obtained from Nippon Zeon Co. Ltd. (Tokyo, Japan). It was reported to have epoxy cure site and was made from ethyl acrylate monomer. Tetraethoxysilane (TEOS, density = 930 kg/m^3) was procured from Acros Organics (USA). Tetrahydrofuran (THF, 99% pure) was purchased from Merck (India). The precipitated silica (Ultrasil VN_3, particle size range = 40–100 nm, oil absorption = 2.4 g/kg, pH = 6) was supplied by Bayer AG (Germany). Benzoyl peroxide (BPO, 97% purity) was purchased from Aldrich Chemicals (USA). Hexamethylenediamine carbamate (HMDC, DIAK#1) was supplied by Nicco Corp. Ltd. (India). Ammonium benzoate (AmBz) was prepared in the laboratory by reacting ammonium hydroxide and benzoic acid in 1:1 molar ratio in a water bath at around 60°C for 30 min. The salt formation was confirmed by Fourier transform infrared spectroscopy as well as by studying its solubility. Deionized water and concentrated hydrochloric acid of laboratory grade were obtained from indigenous sources.

TABLE I
Compositions of the Hybrid Composites

Sample designations	TEOS (wt %)	ppt Silica (wt %)	BzO (wt %)	(AmBz + HMDC) (wt %)	Appearance of the films
ACM					Transparent
ACM10	10				Transparent
ACM20	20				Transparent
ACM30	30				Transparent
ACM40	40				Transparent
ACM50	50				Transparent
ACMs 10		10			Opaque
ACMs 20		20			Opaque
ACMs 30		30			Opaque
ACM B			0.2		Translucent
ACM B10	10		0.2		Translucent
ACM B20	20		0.2		Translucent
ACM B30	30		0.2		Translucent
ACM B40	40		0.2		Translucent
ACM B50	50		0.2		Translucent
ACM D				2.5 + 1.5	Translucent
ACM D10	10			2.5 + 1.5	Translucent
ACM D20	20			2.5 + 1.5	Translucent
ACM D30	30			2.5 + 1.5	Translucent
ACM D40	40			2.5 + 1.5	Translucent
ACM D50	50			2.5 + 1.5	Translucent

Preparation of hybrid composites by sol-gel technique

The desired amount of ACM was dissolved in THF solvent. A proportion of the rubber to solvent was maintained at about 1 : 10 all throughout the experiment to retain the uniform viscosity of the reaction medium. TEOS, deionized water, and concentrated HCl as catalyst, in the molar ratio of 1 : 2 : 0.06,[15] were throughly mixed by vigorous stirring for 15 min and then the mixture was added to the rubber solution under stirring conditions at ambient temperature. The proportion of TEOS was from 0 to 50 wt % of the ACM. Beyond 50 wt % TEOS, macrophase separation occurred. The formulations used in this study are given in Table I. The precursor solution for preparing the composites was stirred for 30 min and then poured over a uniform and thoroughly cleaned glass plate. The initial evaporation of the solvent was carried out under controlled conditions for 24 h, and then, in the next phase, further evaporation for 4 days was allowed to remove the residual solvent and byproducts (water and ethanol). The optimum gelling time was taken when practically *no* weight variation of the hybrid composites was noticed. All the films were transparent in appearance. For comparison, composites

were also prepared with precipitated silica up to 30 wt % of its loading (beyond which the resultant film lost its homogeneity). The precipitated silica was initially dried at 120°C for 24 h and then dispersed in the ACM solution. All the composite films with precipitated silica were opaque and completely white in color. To crosslink the rubber phase, curatives were added to the solvated rubber. The two different curatives systems used in this study were BPO and a mixed crosslinked system comprising AmBz and HMDC, following an earlier work on acrylic rubber in our laboratory.[16] Optimization of the doses of different curatives (Table I) was carried out by studying the maximum gel content in THF.

Addition of curatives was made only after complete mixing of TEOS, water, and HCl with solvated ACM for 30 min. The crosslinkers were dispersed under ambient conditions and then stirred for another 30 min for homogenous mixing. The films were cast over a plain glass plate as before and kept for controlled solvent evaporation for 24 h. In the next phase, peroxide-containing composite films were kept in the oven at 70°C for 2 h for curing, whereas the samples having mixed crosslinked system were cured at 170°C for 30 min. The above cure times were optimized from the maximum gel content values.

Characterization of hybrid composites

Infrared (IR) spectroscopy

The infrared (IR) spectra of the cured and uncured hybrid composite films were recorded with a Nicolet Nexus FTIR spectrophotometer in ATR mode by using 45° KRS5 prism at room temperature. The samples were scanned from 2000 to 600 cm^{-1} with a resolution of 4 cm^{-1}. All the spectra were taken after an average of 32 scans for each specimen.

Transmission electron microscopy (TEM)

Transmission electron microscopic studies were performed by using a TEM (model C-12, Philips) on very thin films of the hybrid composites, cast directly over the copper grids of 300-mesh size. The acceleration voltage was 120 kV. The images presented for this study were of identical magnification of ×80,000.

Scanning electron microscopy (SEM) and X-ray silicon mapping

The dispersion of silica particles in the ACM matrix was observed through microscopic investigations with a JEOL JSM 5800 scanning electron microscope. The samples were sputter coated with gold to avoid the artifacts associated with sample charging. The acceleration voltage was 20 kV. All the images were taken in a uniform magnification of ×10,000. For precipitated silica-containing samples, a magnification of ×200 was used. The X-ray silicon mapping of the hybrid composite films were recorded in an Oxford EDAX system, attached to the microscope. The magnification used in this case was ×2000.

Dynamic mechanical thermal analysis (DMTA)

Dynamic mechanical thermal characteristics of the hybrid composite films were evaluated in a DMTA IV (Rheometric Scientific) under tension mode. The experiments were carried out at a frequency of 1 Hz. The measurements were taken from −80 to 100°C at a heating rate of 2°C/min. The data were analyzed by using RSI Orchestrator application software on an ACER computer attached to the machine. The storage modulus and loss tangent (tan δ) were measured for all the samples under identical conditions.

Determination of mechanical properties

The mechanical properties of the composites were evaluated with a universal testing machine (UTM, Zwick 1445) on tensile specimens, punched out from the cast films by using ASTM Die C. The mechanical tests were carried out as per ASTM D 412-99 method at 25 ± 2°C at a crosshead speed of 500 mm/min. The average value of three tests was reported for each sample.

Thermogravimetric analysis (TGA)

Thermogravimetric analysis of the composites was performed by using a DuPont TGA instrument (Model no. 2000) from ambient temperature to 800°C at a programmed heating rate of 20°C/min in nitrogen atmosphere. A sample weight of ~ 10 mg was taken for all the measurements. The weight loss against temperature was recorded.

Swelling behavior

Swelling behavior of the cured and the uncured ACM/silica hybrid composites was studied with the sample films in THF under ambient conditions. Equilibrium swelling weight of the films was determined after 72 h.

RESULTS AND DISCUSSION

Appearance of all the hybrid composite films prepared by sol-gel technique in this study is transparent (Table I). The optical transparency is an indication of

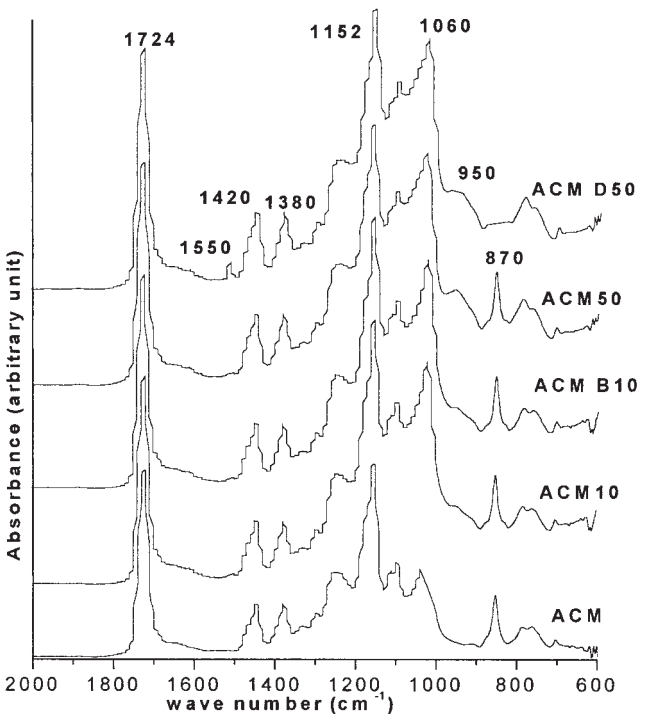

Figure 1 FTIR spectra for representative cured and uncured ACM/silica hybrid composites.

homogenous nanophase dispersion of the inorganic constituents in the polymer matrix. When the macroscopic phase separation in the system occurs, the products appear opaque because of the large domain size of the distributed inorganic moieties that diffract light. The composites of ACM with precipitated silica are opaque at all proportions.

Infrared spectroscopic analysis (FTIR)

The FTIR spectra of the representative cured and uncured hybrid composites along with pure ACM are shown in Figure 1 and the characteristic peaks are assigned in Table II. The strong absorption bands at 1724 and 1152 cm^{-1} corresponding to ester carbonyl group and asymmetric C—O—C stretching are found to be present in the pure ACM as well as in all the hybrid composites. The C—H bending and C—H deformation at 1446 and 1380 cm^{-1} are also noticed for the same. The symmetric C—O—C stretching absorption due to the ester groups in the acrylic rubber is probably interfering with the Si—O—Si stretching in the region of 1060 cm^{-1} in the hybrid composites. Asymmetric stretch for Si—O—C linkage is also likely to be present in this region, which is due to some unhydrolyzed TEOS adsorbed in the composites. Associated symmetric stretch for Si—O—C at around 870 cm^{-1} may overlap with the C—O—C stretch due to the epoxy cure sites present in the rubber. Some residual solvents may also be entrapped in the matrix, giving rise to absorptions in the same region. Therefore, the intensity of peak at around 870 cm^{-1} was found to be unaffected in the hybrid composites. Appearance of small inflations at 950 cm^{-1} (Si—O stretch) for the hybrid composites indicates the presence of some silanol (Si—O—H) groups in the samples. No shift in peak position for carbonyl absorption in all the hybrid composites, as shown in Figure 1, reveals the homogenous dispersion of the inorganic phases over the organic matrix without any substantial interaction occurring between them.[15] This conclusion is further supported from the complete dissolution of the uncured hybrid composites in THF under ambient temperature.

For amine-cured sample (ACM D10, Fig. 1), the absorption peak at 870 cm^{-1} is absent because of the crosslinking reaction taken place within the systems. It also suggests that the residual solvents and the adsorbed TEOS were removed at the curing temperature of the rubber. The small absorption peak at 1550 cm^{-1} for N—H bending vibrations implies the presence of unreacted amines in the same sample. Infrared spectroscopy of peroxide-cured composites, ACM B10, virtually shows no difference from that of the uncured ACM10 composite.

Microscopic observations

Figure 2(a–c) shows the TEM micrographs of the organic–inorganic hybrid composites prepared with 10, 30, and 50 wt % of TEOS, respectively. The presence of silica particles as dark regions dispersed within the ACM matrix is apparent. The sample containing 10 wt % of TEOS [ACM10, Fig 2(a)] exhibits discrete spherical silica particles with an average diameter of 20 nm, dispersed over the ACM matrix. However, some connectivity among the silica particles is observed as the TEOS concentration is increased from 10 to 50 wt %.

TABLE II
Assignments of Characteristic Absorption Peaks from the FTIR Spectra of the Hybrid Composites

Peak value (cm^{-1})	Peak assignments
1724	Ester C═O stretch
1550	N—H bending
1446	C—H bending
1380	C—H deformation
1152	Asymmetric C—O—C stretch for ester
1060	Si—O—Si stretch
	Asymmetric Si—O—C stretch
950	Si—OH stretching
870	C—O—C stretch for epoxy
	Symmetric Si—O—C stretch

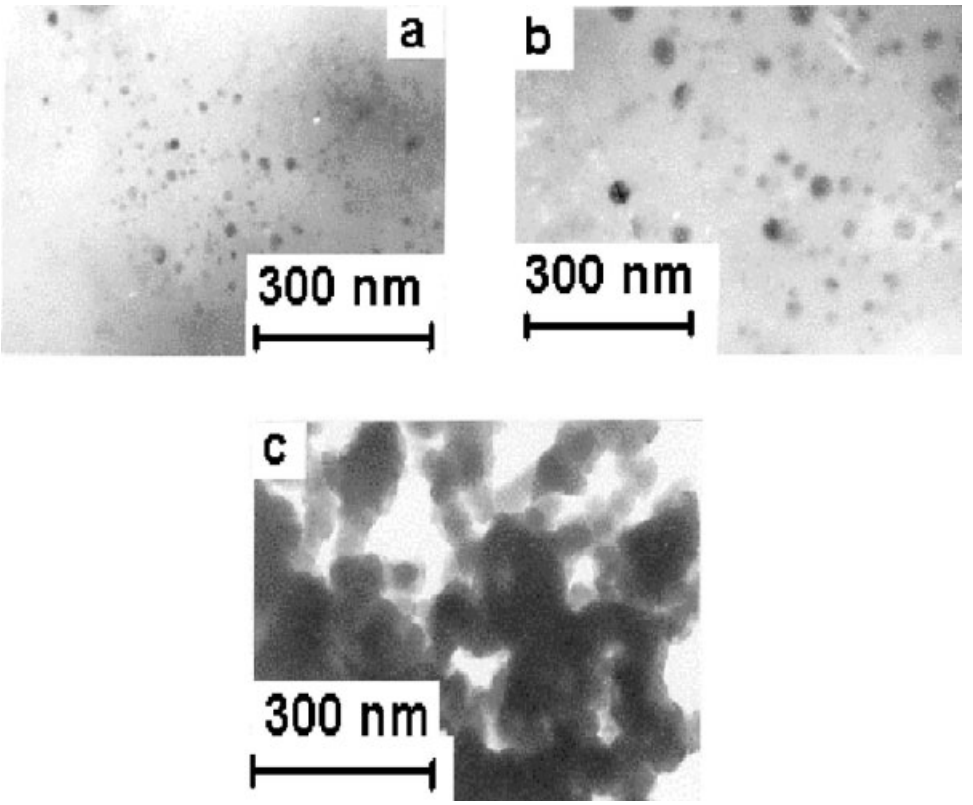

Figure 2 Transmission electron micrographs with magnifications of ×80,000 for (a) 10 wt % TEOS loaded, (b) 30 wt % TEOS loaded, and (c) 50 wt % TEOS loaded ACM hybrid composites.

Moreover, with increasing loading of TEOS, the average size of the silica particles increases. In ACM30, the average diameter of silica particles is ~ 70 nm, while it has increased to about 90 nm in ACM50 composites [Fig. 2(b, c)]. At higher concentrations of TEOS, discrete silica particles come close to each other, forming a network type of structure, which is evident from the image of ACM50 [Fig. 2(c)]. The dimensions of individual silica particles constituting the network structure are hard to invade further, because of the instrumental limitations.

The SEM image of the representative ACM50 hybrid composite is shown in Figure 3(a). The micrograph gives evidence of the formation of silica network within the ACM matrix in the organic–inorganic hybrid composites. The SEM image is taken in relatively lower magnification than the corresponding TEM images and is therefore capable of viewing a larger area than the TEM counterparts. The SEM photographs elucidate a broader view of the distribution of the silica particles within the composites. Figure 3(b) shows the SEM image of the composite prepared with 10 wt % precipitated silica (ACMs 10). The image clearly exhibits the presence of agglomerated silica particles even with only 10 wt % of silica loading in the sample.

X-ray silicon mapping of ACM10, 30, and 50 hybrid composites is shown in Figure 4(a–c), respectively. The white spots over a dark background indicate the location of silicon atoms within the composites. It is quite evident that the spots become dense with the increase in TEOS content in the composites. At higher concentrations, few white spots are found to join together, indicating local agglomerations.

Analysis of dynamic mechanical properties

Dynamic mechanical property explains the viscoelastic behavior of the hybrid composites. The storage modulus (E') of the uncured hybrids in log scale is plotted against the temperature in Figure 5(a). It was found that, with an increase in TEOS content, the storage modulus increases in the high temperature range. Increase in storage modulus accounts for the reinforcing action of nanosilica network structure present in the rubber matrix. This is further elucidated by the storage modulus values at the three different temperatures: −40°C [below glass transition temperature (T_g)], at T_g (the peak maxima value of the tan δ curve), and +25°C (above T_g) reported in Table III. The hybrid composites with higher silica content exhibit higher modulus, especially at higher tempera-

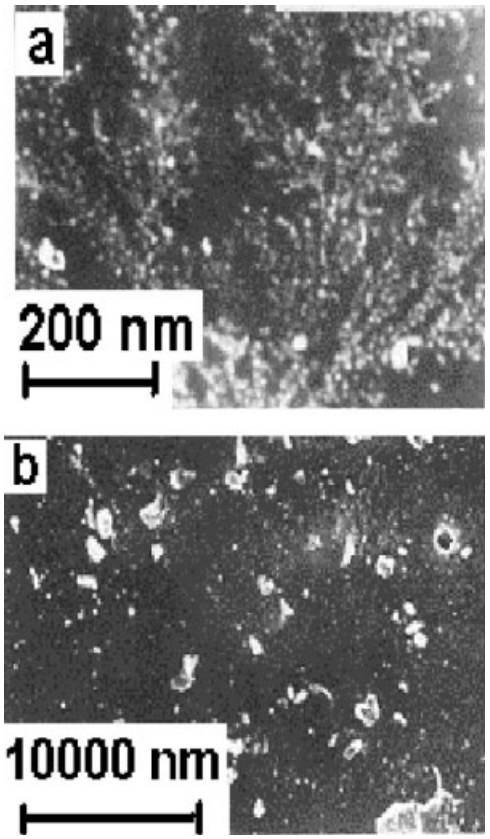

Figure 3 Scanning electron micrographs for (a) ACM hybrid composite modified with 50 wt % TEOS at magnification ×10,000 and (b) ACM sample with 10 wt % ppt. Silica at magnification ×200.

tures. The difference between these values is highest at 25°C. Incorporation of 50 parts of TEOS improves the storage modulus at 25°C by 21% Figure 5(b) shows the tan δ plots for the uncured hybrid composites in the temperature range of −80 to 100°C. It is quite evident that the peak height gradually reduces (Table III) and the peak broadens with the increase in the TEOS percentages in the organic–inorganic hybrids. The T_g of the composites shifts towards higher temperature regions with an increase in TEOS loading. Figure 5(c) shows the increase in glass transition temperature and the decrease in peak maxima values for the tan δ plots with various doses of TEOS loading in the hybrid composites. The downward shift in peak maxima value exhibits a sharp decrease at 20 and 40 wt % of TEOS loading in the sample. On the other hand, the change in the T_g value with respect to TEOS loading in the composites increases sharply with TEOS concentration. The effect of reinforcing filler on the reduction of tan δ and shifting of T_g towards higher temperature was discussed in the literature.[17] The T_g value increases from −24°C (neat ACM) to −5°C (ACM50), as evident from Table III.

Analysis of mechanical properties

The mechanical properties of both uncrosslinked and crosslinked hybrid composite films have been determined. Tensile stress–strain curves for the uncured rubber composites are shown in Figure 6(a). The tensile strength, tensile modulus at 300% elongations, and elongations at break calculated from these curves are registered in Table IV. The gum ACM shows very poor tensile strength of only 0.27 MPa. In the hybrid composites, the strength increases with the increase in the TEOS content. For ACM50, the tensile strength

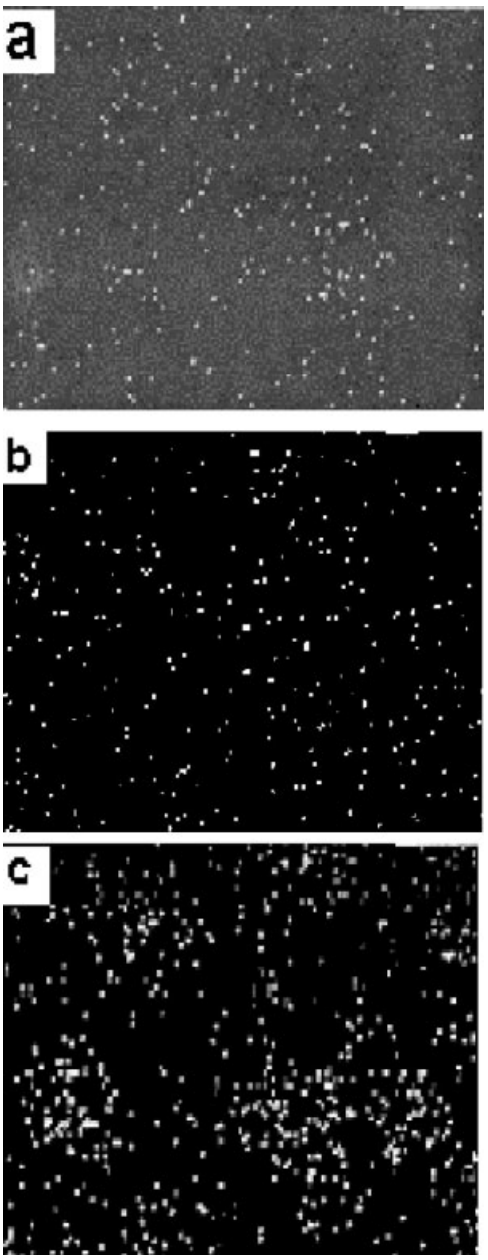

Figure 4. X-ray silicon mapping for (a) 10 wt % (b) 30 wt % and (c) 50 wt % TEOS loaded ACM hybrid composites (magnification, ×2000).

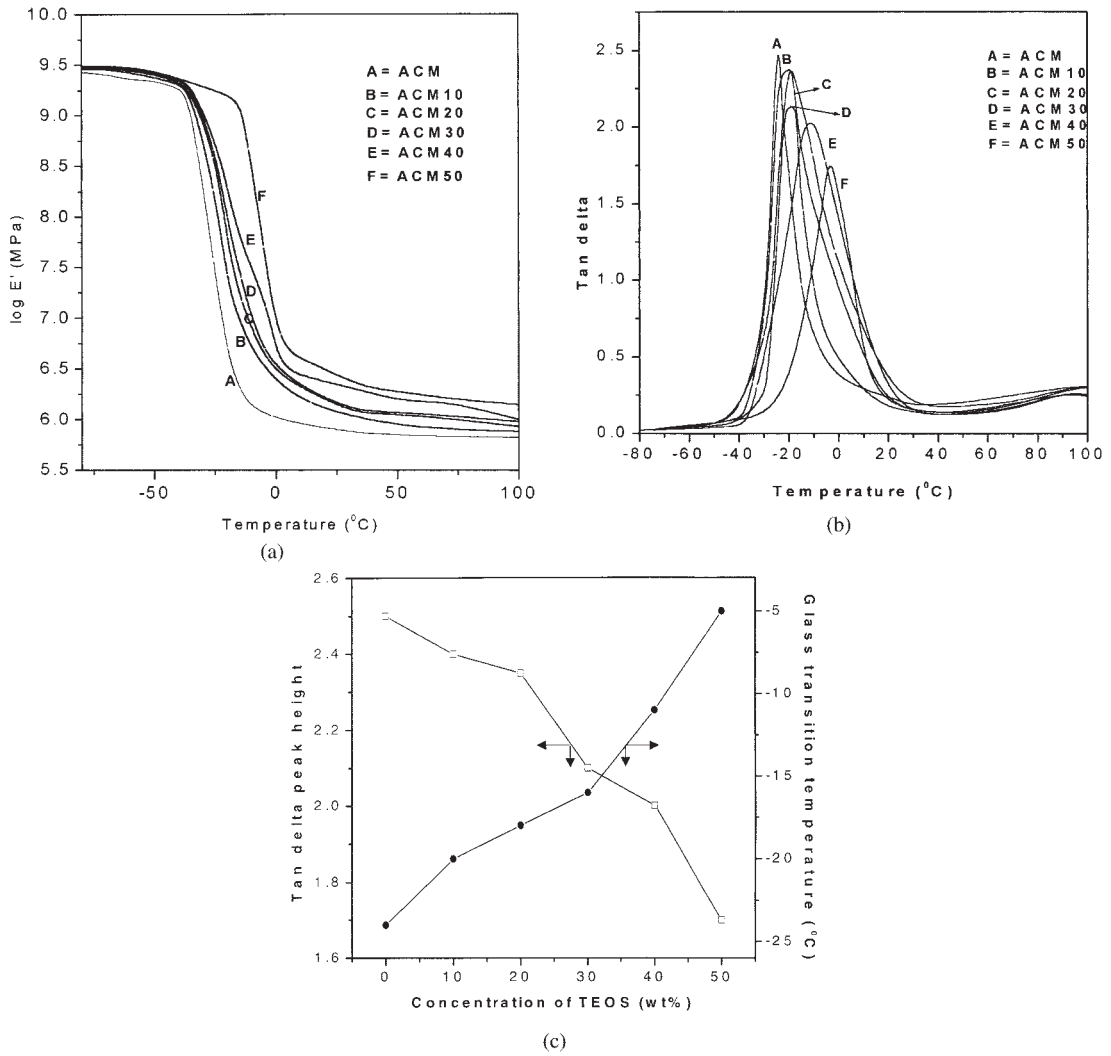

Figure 5 (a) Storage modulus plots for uncured ACM hybrid composites. (b) Tan delta plots for uncured ACM hybrids composites. (c) Variations of glass transition temperatures and loss tangent peak maxima with varying concentrations of TEOS in the hybrid composites.

value is recorded to be 1.5 MPa, which is more than 457% higher than that of pure ACM rubber. All the hybrid composites also exhibit a gradual increase in 300% modulus values, which are virtually very close to their corresponding tensile strength values. Bhowmick et al.[18] used a model equation to interpret the filler–polymer interactions within the filled rubber composites

$$E_f/E_0 = ae^{b\phi} \tag{1}$$

where E is the Young's modulus and the subscripts f and 0 indicate filled and unfilled polymer samples. a and b are the constants at a particular strain level and temperature. ϕ denotes the volume fraction of the fillers in the composites. In log scale, eq. (1) takes the form

$$\ln E_f/E_0 = \ln a + b\phi \tag{2}$$

TABLE III
Glass Transition Temperatures, Storage Modulus, and tan δ Values for the Uncured ACM Hybrid Composites at Three Different Temperatures

Sample designation	Log E' (Pa)			Tan δ			
	−40°C	T_g	25°C	−40° C	T_g	25° C	T_g (°C)
ACM	9.28	7.24	5.28	0.12	2.54	0.24	−24
ACM10	9.34	7.30	5.99	0.15	2.40	0.22	−20
ACM20	9.35	7.40	6.10	0.09	2.38	0.20	−18
ACM30	9.37	7.51	6.15	0.06	2.00	0.17	−16
ACM40	9.38	7.71	6.39	0.04	1.80	0.16	−11
ACM50	9.39	7.77	6.41	0.08	1.67	0.15	−5

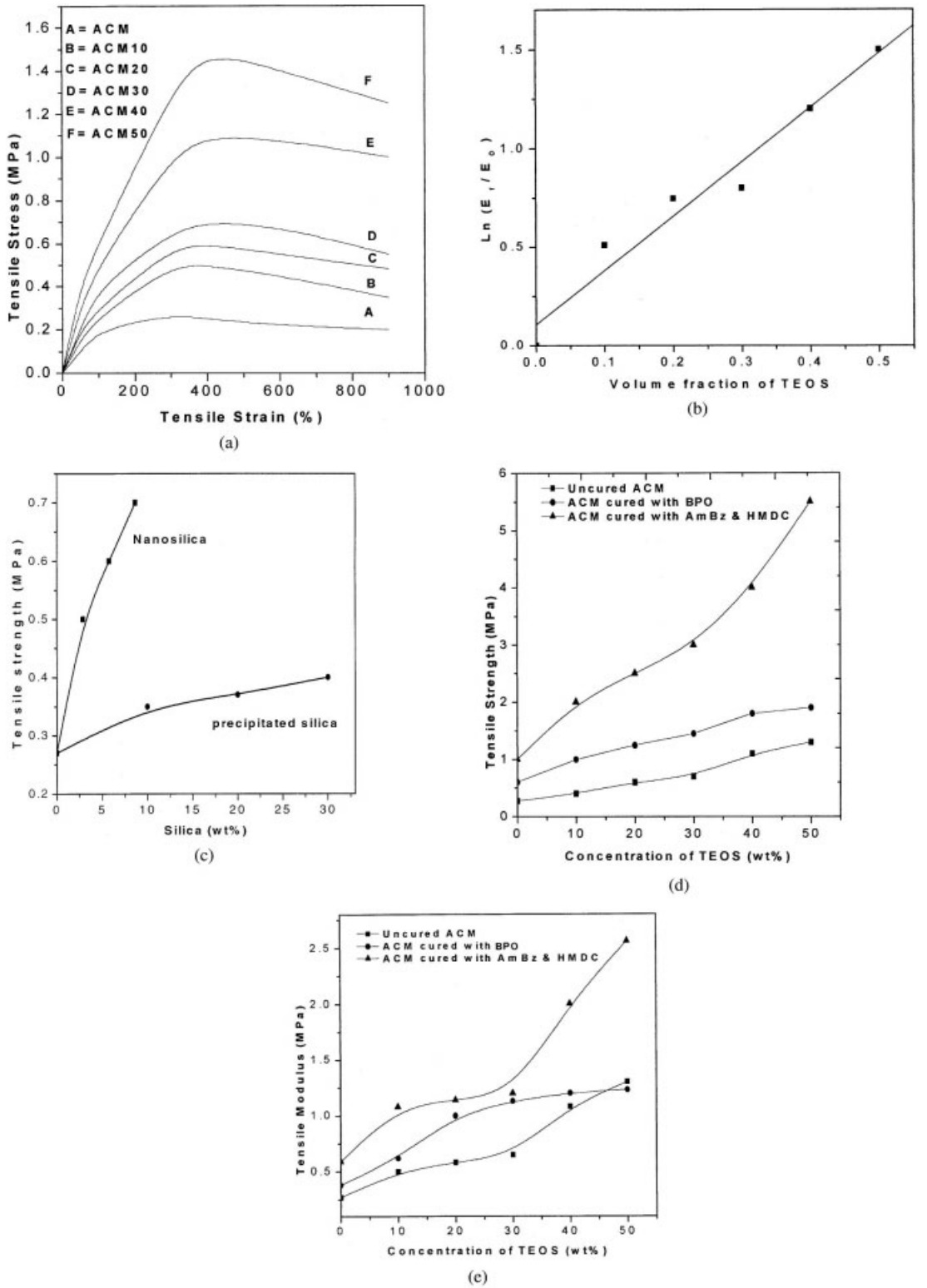

Figure 6 (a) Tensile stress–strain plots of ACM/silica hybrid composites. (b) Plot of logerithimic ratio of Young's modulus for the uncured ACM/silica hybrid composites against volume fractions of TEOS added. (c) Comparative plots of tensile strength values for nanosilica and ppt silica containing ACM composites at the different levels of silica loading. (d) Comparison of tensile strength values for the cured and uncured ACM/silica hybrid composites with different concentrations of TEOS loading. (e) Comparison of tensile modulus at 300% elongations for the cured and uncured hybrid rubber composites at different levels of TEOS loading.

Values of $\ln E_f/E_0$ against different volume fractions of TEOS in the uncured hybrid composites at an extension ratio of 1.5 is plotted in Figure 6(b). The best fit straight line equation corresponding to the experimental values is

$$\ln E_f/E_0 = 0.22 + 2.43\phi; \quad R^2 = 0.9700 \qquad (3)$$

The values of constants a and b from eq. (3) are determined as 1.24 and 2.43, respectively. Ideally, the value of a is 1.00 for the silica-filled systems[18] but is

TABLE IV
Mechanical Properties Data for ACM/Silica Hybrid Composites

Sample designations	Tensile strength (MPa)	Tensile modulus at 300% (MPa)	EB%
ACM	0.27	0.27	>900
ACM10	0.50	0.50	>900
ACM20	0.60	0.58	>900
ACM30	0.70	0.65	>900
ACM40	1.10	1.00	>900
ACM50	1.50	1.30	>900
ACMs 10	0.35	0.29	>900
ACMs 20	0.37	0.37	>900
ACMs 30	0.40	0.40	>900
ACM B	0.60	0.38	>900
ACM B10	1.00	0.62	>900
ACM B20	1.25	1.00	>900
ACM B30	1.45	1.13	>900
ACM B40	1.80	1.20	>900
ACM B50	1.90	1.23	>900
ACM D	1.00	0.59	800
ACM D10	2.00	1.08	830
ACM D20	2.50	1.14	790
ACM D30	3.00	1.20	760
ACM D40	4.00	2.00	690
ACM D50	5.50	2.56	650

little higher in the present case. The filler–polymer interactions within the composite were described by the constant b.[18] Substantially high slope ($b = 2.43$) in this case indicates higher interactions occurring between the nanosilica particles and the acrylic rubber matrix. The nature of this interaction was discussed under infrared spectroscopic analysis of the hybrid composites. The same rubber did not show much improvement in the mechanical properties when mixed with the precipitated silica. The comparative plots of tensile strength values against concentration of TEOS and externally added precipitated silica in weight percentage are given in Figure 6(c). Corresponding model equations are given as

$$Y = 0.27 + 0.05X - 0.001X^2; \quad R^2 = 0.9916 \quad (4)$$

$$Y = 0.27 + 0.007X - 1.25 \times 10^{-4}X^2; \quad R^2 = 0.9735 \quad (5)$$

Equation (4) corresponds to the nanosilica hybrid composites, whereas eq. (5) is for the hybrids containing precipitated silica. The improvement in tensile strength in the case of *in situ* silica hybrids compared to the precipitated silica hybrids can also be explained from the morphological viewpoints. In the silica composites, generated *in situ,* the nanolevel mixing of silica particles and the formation of strong Si—O—Si network within the ACM phase causes greater reinforcement in the rubber matrix, and hence, improvement of tensile strength and modulus occurred. In the case of the precipitated silica-filled composites, the bigger sized silica particles do not provide higher surface area for interactions such as *in situ* silica, and hence, are not as effective as the former. However, all the composites, irrespective of being prepared with nanosilica or precipitated silica, showed very high elongations (>900%).

The crosslinked samples exhibit further improvements in both tensile strengths and 300% modulus values (Table IV). The enhancement is higher for the composites cured with the mixed crosslinked system when the results are compared with those prepared by using peroxide. For example, ACM50 hybrid composite when cured with BPO gives 27% increment in tensile strength, whereas the same sample produces 267% improvement when cured with AmBz and HMDC system. The tensile strength and 300% modulus values for the cured and the uncured hybrid composites are plotted in Figure 6 (d, e). The nature of the plots of tensile strength against TEOS concentrations for the uncured ACM and ACM cured with BPO is very similar. Both increase linearly with increasing concentrations of TEOS. However, ACM cured with AmBz and HMDC displays sharp increase in tensile strength in the initial stages, up to 30% TEOS loading, beyond which there is an exponential increase in the strength. The modulus of the same samples exhibits very similar behavior. It is interesting to note that there is about 100% increase in tensile modulus of ACM cured with AmBz and HMDC for ACM50, whereas virtually no change for the sample is noted when cured with BPO, as compared to the gum-cured rubber samples. It was observed that the equilibrium swelling indices, under ambient conditions, in THF, is the same for all the hybrid composites cured with AmBz and HMDC (the equilibrium swelling index is around 480). Similar results are also noted for the BPO-cured samples (equilibrium swelling index for this system is around 550). This indicates that increased value at high TEOS/silica concentration is due to an increasing number of particles, their uniform distribution, and favorable kinetics of nanosilica formations and not due to the change in the crosslinking density. It may be mentioned here that the rubber in the uncured hybrid samples completely dissolves in THF and does not show any formation of gel.

The curing efficiency of peroxides is lower than that of ammonium benzoate/HMDC system.[16] Peroxide-cured samples show higher swelling than the mixed crosslinked samples, indicating lower crosslink density. This is further evident from the tensile strength as well as the elongation at break percent values. Peroxide-cured composites show elongations >900%,

TABLE V
Thermogravimetric Data for ACM Hybrid Composites

Sample designations	T_{10} (°C)	T_{max} (°C)	Rate of maximum degradation (wt % loss/min) at T_{max}	% Residue at 800°C
ACM	375	403	51.5	4.00
ACM10	380	405	48.8	7.00
ACM30	380	405	44.1	14.0
ACM50	380	405	25.2	22.0
ACM B10	382	405	45.4	7.00
ACM D30	387	405	40.0	14.0

whereas the mixed crosslinked composites give elongation <900%.

Thermogravimetric analysis

Table V lists the thermogravimetric data for the representative crosslinked and uncrosslinked hybrid composites. The thermal degradation temperature corresponding to an initial 10% weight loss is the same for the hybrid composite films containing 10, 30, and 50 wt % of TEOS, respectively. These values are marginally higher than the corresponding neat rubber specimen. It is probably due to the lack of chemical interactions at the interfaces of the organic and inorganic moieties within the composite films, as discussed earlier. ACM B10 hybrid composite shows lesser improvement in the initial degradation temperature over ACM10, while the improvement is higher in the case of ACM D30 over the uncured hybrid sample ACM30, as is evident from Table V. This level of difference is obtained because of the effective curing of the rubber phase by the mixed crosslinkers than the peroxide. No variation is observed in the maximum degradation temperatures for the representative composite samples (Table V), although nanolevel dispersion of silica does improve the rate of thermal degradation for the same at the maximum degradation points. An improvement in the rate of thermal degradation as high as 100% is registered for ACM50 compared to the virgin rubber. However, ACM10 and ACM30 hybrid composites do not show much improvement in rate when they are crosslinked. The percentage residues at 800°C increase along with the increase in silica content in the composites.

Table VI reports the amount of silica obtained practically after degrading the composites at 800°C. It is calculated by subtracting the residues obtained for pure ACM from the residues of the hybrid composites. When these results are compared with the theoretical silica content of the samples, based on the initial amount of TEOS added, the former is found to be less than the theoretical amount. The difference in the amount of experimentally obtained silica from its theoretical amount increases with higher TEOS loading. This is due to the incomplete hydrolysis occurring in TEOS, as already mentioned in the infrared spectroscopic analysis.

CONCLUSION

Acrylic rubber/silica organic–inorganic hybrid nanocomposites were successfully synthesized by using sol-gel technique. TEM study shows the formation of nanosilica particles of average dimensions of 20–90 nm, distributed over the rubber matrix. SEMs exhibit the formation of silica network at the higher loading of TEOS in the hybrid composites. X-ray silicon mapping gives uniform distribution of silica particles within the rubber matrix. FTIR spectroscopic analysis indicates lack of chemical interactions at the organic–inorganic interfaces. The hybrid composite films are optically clear because of the existence silica particles in the nanometer level. In the case of the precipitated silica composites, there is clear evidence of agglomerations of the filler particles, which render the film opaque. Dynamic mechanical properties show mechanical reinforcements within the hybrid composites. The TEOS loaded uncured samples exhibit higher modulus all throughout the experimental temperature range. Progressive positive shifts in glass transition temperatures as well as the reduction in peak heights of the loss tangent indicate physical adsorptions of the fillers over the rubber chains, thereby restricting the polymer chain movements. Mechanical properties of the composites are also improved, as the TEOS concentrations are increased. ACM50 composite registers 457% higher tensile strength than the virgin rubber. On curing the rubber phase, with either BPO or AmBz and HMDC, the tensile strength is further increased, although BPzO-cured samples show lesser improvements than the corresponding mixed crosslinked samples. The tensile modulus at 300% elongations of the uncured hybrid composites is comparable with the BPO-cured samples, while the samples cured with AmBz and HMDC combinations give better results. Thermal stability of the hybrid composites is not im-

TABLE VI
Quantification of wt % Silica Obtained Theoretically and Practically from Hydrolysis of %TEOS from Thermogravimetric Analysis

TEOS (wt %)	wt % Silica (theoretical)	wt % Silica (practical)
10	4.40	3.00
30	13.3	11.0
50	22.1	18.0

proved much, as evident from the thermogravimetric analysis. TGA residue indicates the presence of unhydrolysed TEOS in the composites, which is further supported by the FTIR results.

References

1. Okada, A.; Usuki, A. Mater Sci Eng 1995, 3, 109.
2. Gilman, J. W. Appl Clay Sci 1999, 15, 31.
3. Gilman, J. W.; Jackson, C. L.; Morgan, A. B.; Harris, Jr. R.; Manias, E.; Giannelis, E. P.; Wuthenow, M.; Hilton, D.; Philips, S. H. Chem Mater 2000, 12, 1866.
4. Porter, D.; Metcafe, E.; Thomas, M. J. K. Fire Mater 2000, 24, 45.
5. Zanetti, M.; Lomakin, S.; Camino, G. Macromol Mater Eng 2000, 279, 1.
6. Armes, S. P. Polym News 1995, 20, 233.
7. Godovoski, D. Y. Adv Polym Sci 1995, 119, 79.
8. Yoldas, B. E. J Noncryst Solids 1982, 51, 105.
9. Wei, Y.; Bakthavatchalam, R.; Yang, D. C.; Whitecar, C. K. Polym Prepr 1991, 32, 503.
10. Wei, Y.; Yang, D. C.; Bhakthavatchalam, R. Mater Lett 1992, 3, 261.
11. Wei, Y.; Yang, D. C.; Tang, L. G.; Hutchins, M. K. J Mater Res 1993, 8, 1143
12. Wei, Y.; Yang, D. C.; Tang, L. G. Macromol Chem Rapid Commun 1993, 14, 273.
13. Mark, J. E.; Jiang, C. Y.; Tang, M. Y. Macromolecules 1984, 17, 2613.
14. Roy, S.; Bhowmick, A. K. J Appl Polym Sci 2002, 83, 2255.
15. Huang, Z. H.; Qiu, K. Y. Polymer 1997, 38, 521.
16. Kader, M. A.; Bhowmick, A. K. J Appl Polym Sci 2003, 89, 1442.
17. Thavamani, P.; Bhowmick, A. K. J Mater Sci 1992, 27, 1243.
18. Roy, S.; Shanmugharaj, A. M.; Bhowmick, A. K. J Mater Sci Lett 2002, 21, 1097.